Published in "Superconductor Science and Technology 23(4):
045005, 2010" which should be cited to refer to this work.

The effect of carbon and rare earth oxide co-doping on the structural and superconducting properties of MgB_2

N Ojha[1], V K Malik[2], Rashmi Singla[1], C Bernhard[2] and G D Varma[1,3]

[1] Department of Physics, Indian Institute of Technology Roorkee, Roorkee-247667, India
[2] Department of Physics and Fribourg Centre for Nanomaterials-FriMat, University of Fribourg, Chemin du Musee, CH-1700 Fribourg, Switzerland

E-mail: gdvarfph@iitr.ernet.in

Abstract

Carbon (C) and rare earth oxide (REO) co-doped bulk polycrystalline MgB_2 samples with nominal compositions $Mg_{1-y}(REO)_y(B_{0.95}C_{0.05})_2$ (where $y = 0.00, 0.01, 0.03, 0.05$ and REO = Eu_2O_3 or Pr_6O_{11}) have been synthesized via a solid state reaction route. The XRD results reveal the presence of impurity phases EuB_6 in Eu_2O_3 and PrB_4 and PrB_6 in Pr_6O_{11} co-doped samples along with the main hexagonal phase of MgB_2 and a small amount of MgO. The values of upper critical field (H_{c2}) and irreversibility field (H_{irr}), except H_{c2} of $y = 0.05$ for Eu_2O_3, have been found to increase at all temperatures ($<T_c$) with increasing doping concentration of REO. Improvements in the values of critical current density (J_c) at 10 K for $y = 0.01$ of Eu_2O_3 and $y = 0.01, 0.03$ of Pr_6O_{11} co-doped samples have been observed in high fields (>6.5 T) region. At 20 K enhancement in the high field (>6 T) J_c values for $y = 0.01$, 0.03 of Eu_2O_3 and $y = 0.01$ of Pr_6O_{11} co-doped samples are also reported in the present work. The correlations between the structural characteristics and the observed superconducting properties of the co-doped samples are described and discussed in this paper.

1. Introduction

The MgB_2 superconductor is expected to be a promising material for practical applications because of its high transition temperature (T_c), simple composition, lack of a weak link problem and low cost [1, 2]. Much effort has been made since the discovery of superconductivity in MgB_2 to enhance its superconducting properties, mainly the upper critical magnetic field (H_{c2}), irreversibility field (H_{irr}) and infield critical current density ($J_c(H)$), to the level required for technological applications [3]. Chemical doping has been found very effective in improving the superconducting properties of MgB_2 [3–12]. Although many doping elements and compounds have been used as dopants, the substitution of C for B, using various sources of C such as SiC, C, B_4C, carbon nanotubes and carbohydrates [6, 13–27], has been found very effective in improving the superconducting properties of MgB_2. It is believed that the C substitution for boron enhances H_{c2} while the defects and grain boundaries are responsible for flux pinning [28]. C substitution for boron induces disorder in lattice sites, which leads to enhancement in H_{c2}. The excess carbon and impurity phases in the C doped samples can be embedded within the MgB_2 grains as nano-inclusions, which lead to enhancement in flux pinning. In addition to C, recently it has been observed that doping of rare earth oxides in MgB_2 significantly improve its superconducting properties [9, 30–36]. It has been seen that even though rare earth elements (RE) possess a magnetic moment they do not greatly suppress the superconductivity of MgB_2 [9, 31–35]. For example Chen *et al* [9] have found a significant enhancement in J_c in a low or medium field for 0.5–5.0 wt% Dy_2O_3 doped MgB_2. Cheng *et al*

[3] Author to whom any correspondence should be addressed.

[32] have found no change in crystal structure, T_c or H_{c2} but a significant enhancement in J_c and H_{irr} for 0.1-10% Ho_2O_3 doped MgB_2. A similar study on Pr_6O_{11} doped MgB_2 has shown improvement in J_c and H_{irr} for low level doping ($\sim$1 wt%) and a degradation in performance of MgB_2 for higher doping levels [33]. Our investigations on Pr_6O_{11} and Eu_2O_3 doped MgB_2 samples also revealed improvement in H_{c2}, H_{irr} and $J_c(H)$ without much degradation in T_c [34–36]. Based on the results of various groups it has been found that the possible reasons for improvement in the superconducting properties of rare earth oxide doped MgB_2 are an enhancement in the flux pinning due to magnetic impurity phases within the grains of MgB_2, and lattice distortions. In the case of C doped MgB_2 the enhancement in H_{c2} takes place due to the lattice distortion on C substitution for B. Thus it appears that by simultaneous doping of C and rare earth oxide the superconducting properties of MgB_2 may be further improved. Earlier Flükiger *et al* [29] have shown improvement in $J_c(H)$ and B_{irr} of B_4C and SiC co-doped MgB_2 samples. Therefore, in order to study the combined effect of both C substitution and rare earth oxide doping on the structural and superconducting properties of MgB_2 we have synthesized the Pr_6O_{11}/Eu_2O_3 and C co-doped MgB_2 samples via solid state reaction route. The composition of C in MgB_2 is generally expressed by the formula $Mg(B_{1-x}C_x)_2$ and the best results have been found for $x = 0.05$ [12, 37, 38]. Hence, in the present case, we have synthesized samples with nominal compositions $Mg_{1-y}(REO)_y(B_{0.95}C_{0.05})_2$ (where $y = 0.00, 0.01, 0.03, 0.05$ and REO = Eu_2O_3 or Pr_6O_{11}) and studied the variation in the structural and superconducting properties (H_{c2}, H_{irr} and $J_c(H)$) with the composition of rare earth oxide in the samples.

2. Experimental details

The rare earth oxide and C co-doped MgB_2 samples have been synthesized with nominal compositions $Mg_{1-y}(REO)_y(B_{0.95}C_{0.05})_2$ (where $y = 0.00, 0.01, 0.03, 0.05$ and REO = Eu_2O_3 or Pr_6O_{11}) via a solid state reaction route. Appropriate amounts of Mg, B, graphite and Eu_2O_3, or Pr_6O_{11}, were mixed and ground in an agate mortar. The resulting powder was pelletized in the form of rectangular pellets. The pellets were sintered at $\sim$850 °C in flowing Ar for $\sim$3 h and finally cooled down to room temperature by switching off the furnace. Henceforth, the undoped samples and co-doped samples with Eu_2O_3 compositions $y = 0.0, 0.01, 0.03$ and 0.05 will be represented as MB, MBC, MBCE1, MBCE3 and MBCE5, respectively. Similarly, Pr_6O_{11} co-doped samples with compositions $y = 0.01, 0.03$ and 0.05 will be represented as MBCP1, MBCP3 and MBCP5, respectively. The samples were characterized by x-ray diffraction (XRD) for phase identification. The microstructural properties were studied by FESEM. The resistivity transitions in fields up to 8 T were measured by a Physical Properties Measurement Systems (PPMS-Quantum Design 6000). H_{c2} and H_{irr} were estimated from the resistive transition curves using the criteria 90% and 10% of the normal state resistivity, respectively [39]. The magnetization of samples was measured at 10 and 20 K using PPMS. The magnetic J_c values were calculated from the width of the magnetization loop ΔM using the formula $J_c = 30\Delta M/d$, where 'd' is the average grain size [40].

3. Results and discussion

Figure 1 shows the XRD patterns of the co-doped and undoped MgB_2 samples synthesized in the present work. The XRD patterns of samples MB and MBC reveal the presence of a dominant hexagonal crystal structure of MgB_2 with only a small amount of impurity phase MgO. On the other hand, XRD patterns of Eu_2O_3 co-doped MgB_2 samples show, besides MgO, the presence of an impurity phase EuB_6 and the intensities of the peaks of this phase increase with increasing doping level of Eu_2O_3 in the samples. In addition to the peaks of impurity phases EuB_6 and MgO, the peak of a EuC_2 impurity phase is observed at $2\theta \sim 26°$ in the XRD patterns of Eu_2O_3 co-doped samples (see figure 1(a)). The impurity phase EuC_2 forms due to reaction of Eu and C present in the reaction mixture. The intensity of this peak, however, decreases with increasing doping level of Eu_2O_3. As we have synthesized the samples with fixed C concentration, the ratio of C and Eu in the sample decreases with increasing Eu_2O_3 content in the samples. Possibly due to this there is decrease in the intensity of the EuC_2 peak with increasing Eu_2O_3 content in the sample. In Pr_6O_{11} co-doped MgB_2 samples, besides MgO, impurity phases PrB_6 and PrB_4 have been detected through XRD results. Like the Eu_2O_3 co-doped samples in this case the intensities of these impurity phases also increase with increasing doping level of Pr_6O_{11}. Moreover, comparison of the XRD patterns of Eu_2O_3 and Pr_6O_{11} co-doped samples reveals that the MgO peaks are more intense in the XRD patterns of Pr_6O_{11} co-doped samples as compared to the corresponding Eu_2O_3 co-doped ones. This is possibly due to more oxygen atoms in the dopant Pr_6O_{11} as compared to the dopant Eu_2O_3. From the XRD patterns it can be seen that the intensity of the MgO peak increases with increasing doping concentration of Pr_6O_{11} in the sample. This result shows that the MgO content in the sample increases with increasing doping concentration of Pr_6O_{11} in the sample. The peaks of all the impurity phases have been marked in figure 1. The lattice parameters calculated from the XRD results are given in table 1(a) and (b) for Eu_2O_3 and Pr_6O_{11} co-doped samples, respectively. Here it can be seen that the lattice parameters a and c of sample MBC have lower values as compared to sample MB, this confirms the substitution of C for the B of MgB_2. This result is consistent with the previous results of C doped samples [13–15]. Furthermore, the lattice parameters a and c decrease with increasing doping concentration of REO in the samples. As the ionic radii of Eu^{3+} and Pr^{3+} are larger than that of Mg^{2+}, this decrease in the lattice parameters due to the substitution of a rare earth element for the Mg of MgB_2 is ruled out. It can be seen that the FWHM values of the (101) peak increases from 0.294 to 0.481 for Eu_2O_3 doped samples and from 0.294 to 0.581 for Pr_6O_{11} doped samples when values of y increase from 0.01 to 0.05 (see table 1(a) and (b)). This indicates that the crystallinity of the samples decreases with increasing doping level [18, 41]. We have estimated the strain values and crystallite sizes of the samples from the Williamson–Hall plots [42]. It has been

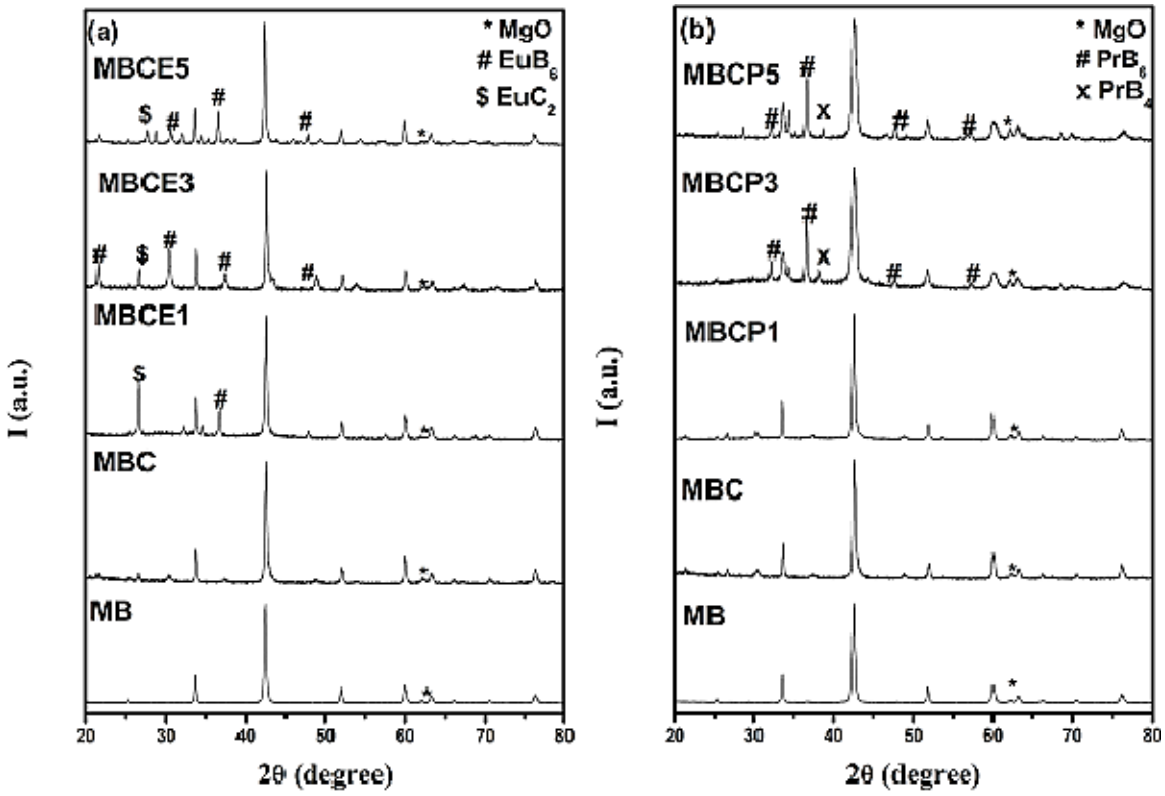

Figure 1. XRD patterns of undoped and co-doped MgB_2 samples.

Table 1. (a) Various parameters of undoped and Eu_2O_3 co-doped MgB_2 samples. (b) Various parameters of undoped and Pr_2O_{11} co-doped MgB_2 samples.

Samples	Lattice parameter (Å) a	c	T_C (K)	FWHM (101)	RRR	Crystallite size (μm)	Vol% of MgO	Strain	A_F
					(a)				
MB	3.0861	3.5222	38.30	0.294	3.35	0.621	1.6	0.025	0.238
MBC	3.0581	3.5180	37.98	0.304	3.12	0.525	2.6	0.026	0.231
MBCE1	3.0551	3.5114	37.81	0.344	3.05	0.483	1.7	0.027	0.224
MBCE3	3.0455	3.5102	37.49	0.377	2.86	0.445	2.0	0.031	0.192
MBCE5	3.0432	3.4950	35.89	0.481	2.70	0.427	3.1	0.035	0.165
					(b)				
MB	3.0861	3.5222	38.30	0.294	3.35	0.621	1.6	0.025	0.238
MBC	3.0581	3.5180	37.98	0.304	3.12	0.525	2.6	0.026	0.231
MBCP1	3.0523	3.5163	35.51	0.362	2.95	0.503	2.9	0.032	0.271
MBCP3	3.0478	3.5129	35.17	0.571	2.74	0.472	3.2	0.038	0.248
MBCP5	3.0472	3.5003	33.33	0.582	2.51	0.468	3.6	0.044	0.185

found that the values of microstrain increase and the crystallite sizes decrease with increasing doping concentration of REO (see table 1(a) and (b)). The increase in strain value with doping is suggestive of a corresponding increase in lattice defect in the co-doped samples, and possibly due to this there is a decrease in the lattice parameters and a reduction in the crystallite size with increasing doping level. The decreased crystallite size helps to enhance the flux pinning, since grain boundaries act as strong pinning centers [18, 43].

The zero resistance ($R = 0$) transition temperatures (T_c) of all the samples have been determined from the R–T measurements (figure not shown here) in zero field, and their values are given in table 1(a) and (b), respectively, for Eu_2O_3 and Pr_6O_{11} co-doped samples. It can be seen that, as usual, T_c decreases on C doping and it further decreases with increasing doping level of REO in the samples. The decrease in T_c on C doping is consistent with the earlier results of C doped MgB_2 samples [24]. However, in the present case, the reduction in the T_c of the C doped sample is less. In the present case, possibly increased disorder is responsible for the decrease in T_c values with increasing REO concentration in the co-doped samples [18, 44–46]. Comparison of the T_c values of Eu_2O_3 and Pr_6O_{11} co-doped samples show higher values of T_c for Eu_2O_3 co-doped samples as compared to the corresponding Pr_6O_{11} co-doped ones. This result is also consistent with the microstrain values of REO doped samples, i.e. the samples

with lower values of microstrain, i.e. less disorder, have higher values of T_c (see table 1(a) and (b)). From the XRD results we have also seen higher MgO content in the Pr_6O_{11} co-doped samples as compared to the corresponding Eu_2O_3 co-doped ones. This may also be responsible for the lower value of T_c for Pr_6O_{11} co-doped samples as compared to the corresponding Eu_2O_3 co-doped ones. From the R–T measurement it has been found that the residual resistivity ratio (RRR = $R_{300\ K}/R_{40\ K}$) values continuously decreases with increasing doping level. This is due to an increase in the amount of impurity phases with increasing doping concentration in the samples. From the table 1(a) and (b) we can see that the RRR values of Pr_6O_{11} co-doped samples have lower values as compared to the corresponding Eu_2O_3 co-doped ones. This result again indicates a higher concentration of impurity phases in Pr_6O_{11} co-doped samples, as suggested by the XRD results. The impurity phases can enhance the electron scattering, and hence a decrease in the RRR value [9]. The effective cross-sectional area, used to estimate the impurity scattering, has been calculated by the equation $A_F = \Delta\rho_{ideal}/(\rho_{300\ K} - \rho_{40\ K})$, proposed by Rowell [47]. $\Delta\rho_{ideal}$ is the ideal change in resistivity from 300 K to 40 K for a fully connected sample and its value is taken to be 7.3 $\mu\Omega$ cm [48]. The calculated values of A_F are given in table 1(a) and (b), respectively, for Eu_2O_3 and Pr_6O_{11} co-doped samples. It can be seen that A_F values of the co-doped samples are smaller than that of the undoped one. This indicates poor connection and high intragrain scattering in the co-doped samples [49]. The poor connectivity due to the presence of impurity phases, such as MgO, PrB_6/EuB_6, PrB_4 and the extra C at the grain boundaries, and high intragrain scattering are responsible for the higher resistivity of the co-doped samples as compared to the undoped one.

The FESEM micrographs of the Eu_2O_3 and Pr_6O_{11} co-doped samples are shown in figures 2 and 3, respectively. For comparison the FESEM micrographs of samples MB and MBC are also given in both figures. From the FESEM micrograph it is clear that the MB sample has a homogeneous microstructure as compared to the co-doped samples. On the other hand, FESEM micrographs of the co-doped samples reveal the presence of clusters of several smaller grains. This is the typical microstructural feature of the doped MgB_2 samples reported earlier [50, 51]. Possibly due to precipitation of the impurity phases at the grain boundaries of MgB_2, some of the grains appear to be well connected together in the co-doped samples. Further, the impurity phases at the grain boundaries inhibit the grain growth, leading to smaller crystallite sizes of the co-doped samples. This result is in conformity with the XRD result.

H_{c2} versus T/T_c and H_{irr} versus T/T_c plots of all the samples synthesized in the present work are shown in figures 4 and 5, respectively. From the plots we see an increase in the H_{c2} and H_{irr} values of sample MBC with respect to sample MB. This result is consistent with the earlier results of C doped samples [52–54]. Moreover, the values of H_{c2} and H_{irr} of co-doped samples as compared to samples MB and MBC further increase with increasing doping concentration of REO in the sample. Whereas the value of H_{c2} continuously increases with the doping concentration of Pr_6O_{11}, it increases only up to $y = 0.03$ for Eu_2O_3 co-doped samples and after this it starts decreasing (see figure 4(a)). The values of H_{c2} of sample MBE5 are, however, higher than those of samples MB and MBC at all temperatures ($<T_c$). On the other hand the values of H_{irr} continuously increase with increasing concentration of REO for both Eu_2O_3 and Pr_6O_{11} co-doped samples. Furthermore, the comparison of the temperature dependence H_{c2} and H_{irr} of Eu_2O_3 and Pr_6O_{11} co-doped samples show higher values of H_{c2} and H_{irr} at all temperatures for the latter dopant. In the present case enhancements of H_{c2} and H_{irr} values of co-doped samples are mainly due to the increased value of lattice strain. We also find a correlation between the FWHM of the (101) diffraction peak and the H_{irr} value as reported by Yamamoto *et al* [55]. This increased H_{irr} value of the co-doped samples is attributed to increased lattice distortions and impurity phases. The higher values of H_{irr} and H_{c2} of Pr_6O_{11} co-doped samples as compared to corresponding Eu_2O_3 co-doped samples are possibly due to more lattice distortion and MgO content in the Pr_6O_{11} co-doped samples, which is evident from the microstrain value and MgO content of the samples given in table 1(a) and (b).

The field dependence of the J_c values of all the samples calculated from the M–H loops, measured at 10 and 20 K, using Bean's critical state model are shown in figure 6. The average crystallite sizes (estimated from the FESEM micrographs) used for the calculation of J_c values are given in table 1. It is seen that the self-field J_c of the doped samples have lower values as compared to that of the undoped samples. The most likely reason for this is increased lattice distortion and impurity phases such as MgO, PrB_6/EuB_6 and unreacted C in the doped samples. In fields >2.5 T we see an improvement in the $J_c(H)$ of sample MBC with respect to MB. This result is similar to earlier results for C doped samples [28, 41, 56]. In the case of Eu_2O_3 co-doped samples at 10 K we see deterioration in the $J_c(H)$ values as compared to sample MBC up to a field ∼7 T, and in fields >7 T there is a slight improvement in the $J_c(H)$ of samples MBCE1 and MBCE3 with respect to sample MBC. As compared to the undoped sample, however, there is an improvement in $J_c(H)$ in fields >6.2 T for all compositions of Eu_2O_3 with much improvement observed for sample MBCE1 (see figure 6(a)). At 20 K we find improvement in the $J_c(H)$ of samples MBC, MBCE1, MBCE3 and a deterioration for sample MBCE5 as compared to MB in fields >2.5 T. Moreover, unlike at 10 K, here we see an improvement in the J_c of samples MBCE1 and MBCE3 as compared to MBC in fields >2.5 T. In the case of Pr_6O_{11} co-doped samples at 10 K and in the field range 2.5–6.5 T, the $J_c(H)$ of the samples MBC, MBCP1 and MBCP3 have nearly the same values, but the values are higher as compared to sample MB. The $J_c(H)$ value of sample MBCP5 has a lower value as compared to sample MB in the field range ∼0–6 T, but there is an improvement in the $J_c(H)$ value of this sample in the field >6 T with respect to the undoped sample (see figure 6(b)). In fields >6.5 T we see an improvement in the $J_c(H)$ values of samples MBCP1, MBCP3 and MBCP5 as compared to those of samples MB and MBC. At 20 K and fields >4.5 T, we see an improvement in the $J_c(H)$ values of all co-doped samples, but in the field range 4.6–6.0 T the

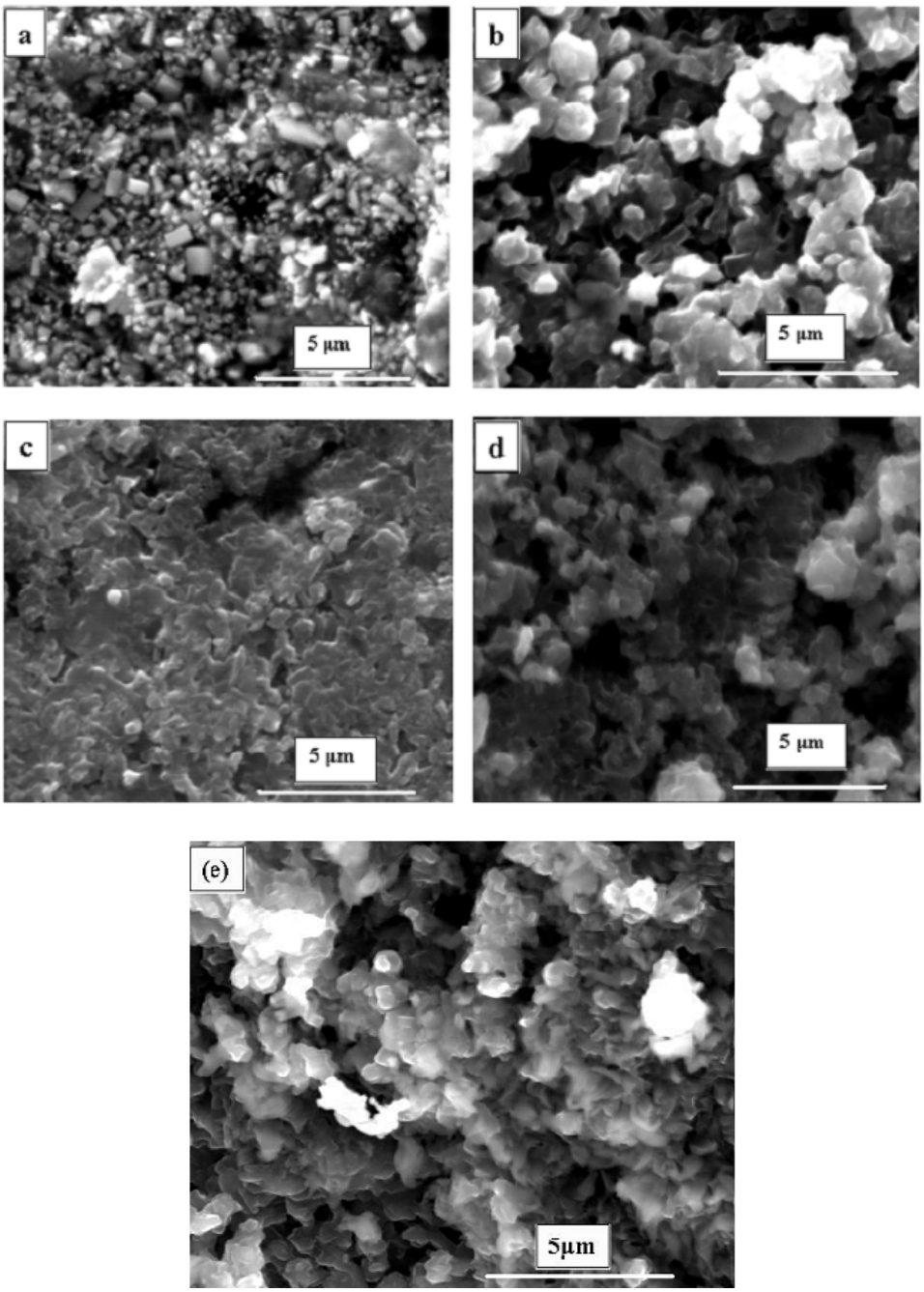

Figure 2. FESEM micrographs of samples MB (a), MBC (b), MBCE1 (c), MBCE3 (d) and MBCE5 (e).

$J_c(H)$ of co-doped samples have lower values as compared to sample MBC. There is, however, a small improvement in the $J_c(H)$ of sample MBCP1 over sample MBC in fields >6.0 T (see figure 6(d)). For comparison, the values of $J_c(H = 0\ \text{T})$, $J_c(H = 5\ \text{T})$ at 10 K and $J_c(H = 0\ \text{T})$, $J_c(H = 4\ \text{T})$ at 20 K of all samples are given in table 2. Thus, based on the present study of the field dependence of J_c, we find that in the case of Eu_2O_3 co-doped samples there is a small improvement in high field (>6.5 T)$J_c(H)$ at 10 K only for sample MBCE1, but at 20 K we see slightly more improvement in a high field (>6 T)$J_c(H)$ for samples MBCE1 and MBCE3 as compared to the $J_c(H)$ value of sample MBC at respective temperatures. On the other hand, in the case of Pr_6O_{11} co-doped samples, we a see slightly greater increase in a high field (>6.5 T)$J_c(H)$ at 10 K for samples MBCP1 and MBCP3 as compared to sample MBC, but at 20 K we see only a small improvement in high field (>6 T)$J_c(H)$ for sample MBCE1 over sample MBC.

In order to study the nature of pinning mechanisms we have calculated the volume pinning force, $F_p = J_c \times H(T)$, of undoped and doped samples at 20 K. The normalized volume pinning force $f_p(h) = F_p/F_{p,max}$ (where $F_{p,max}$ is the maximum pinning force) is plotted against the reduced magnetic field $h = H/H_{irr}$ in figure 7 at 20 K. Here the H_{irr} value has been taken as the field at which J_c becomes 100 A cm^{-2}. It has been observed that if pinning arises due to a grain boundary, f_p follows a $h^{0.5}(1-h)^2$ dependence

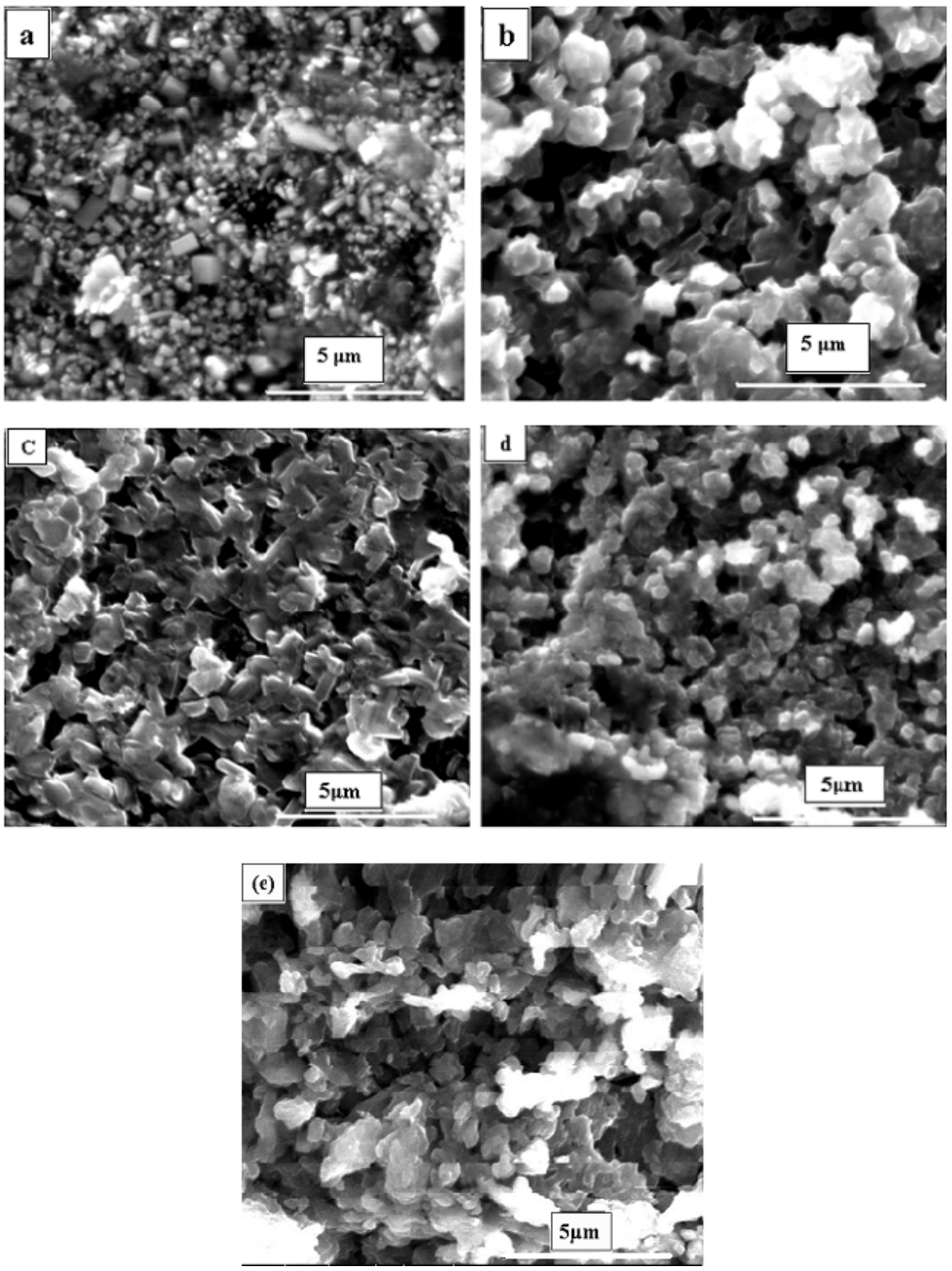

Figure 3. FESEM micrographs of samples MB (a), MBC (b), MBCP1 (c), MBCP3 (d) and MBCP5 (e).

Table 2. Critical current densities of undoped and co-doped MgB_2 samples.

	J_C (A cm^{-2})							
	$Mg_{1-y}(Eu_2O_3)_y(B_{0.95}C_{0.05})_2$				$Mg_{1-y}(Pr_6O_{11})_y(B_{0.95}C_{0.05})_2$			
	10 K		20 K		10 K		20 K	
Samples	0 T	5 T	0 T	4 T	0 T	5 T	0 T	4 T
MB	7.56×10^5	4.83×10^2	4.24×10^5	1.82×10^2	7.56×10^5	4.83×10^2	4.24×10^5	1.82×10^2
$y = 0.00$	2.76×10^5	1.31×10^3	1.74×10^5	4.84×10^2	2.76×10^5	1.31×10^3	1.74×10^5	4.84×10^2
$y = 0.01$	9.88×10^4	1.67×10^2	9.44×10^4	1.03×10^3	1.67×10^5	2.18×10^3	8.50×10^4	2.83×10^2
$y = 0.03$	5.84×10^4	3.31×10^2	6.11×10^4	1.57×10^3	1.29×10^5	1.68×10^3	3.47×10^4	1.27×10^2
$y = 0.05$	2.71×10^4	3.88×10^2	1.92×10^4	19.67	3.91×10^4	2.44×10^2	1.45×10^4	88.31

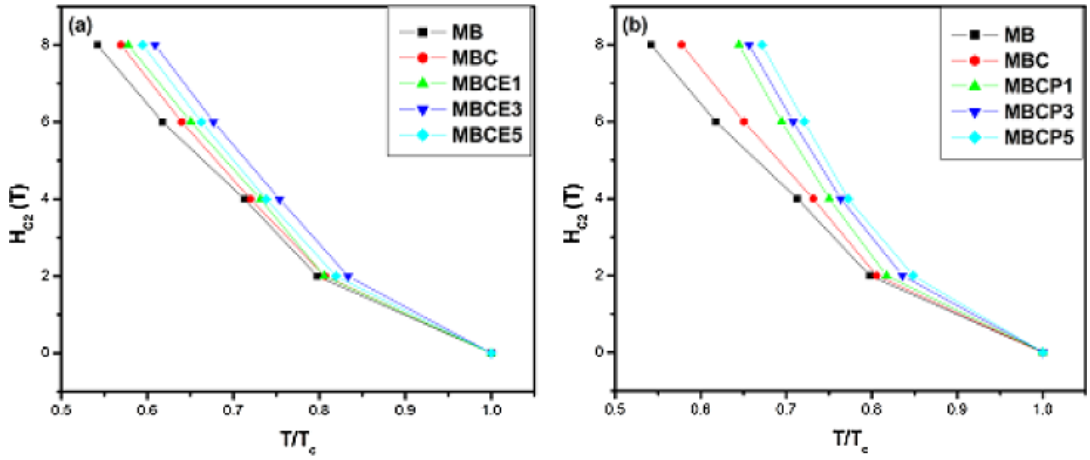

Figure 4. $H_{c2}(T)$ versus T/T_c plots of undoped and co-doped MgB_2 samples.

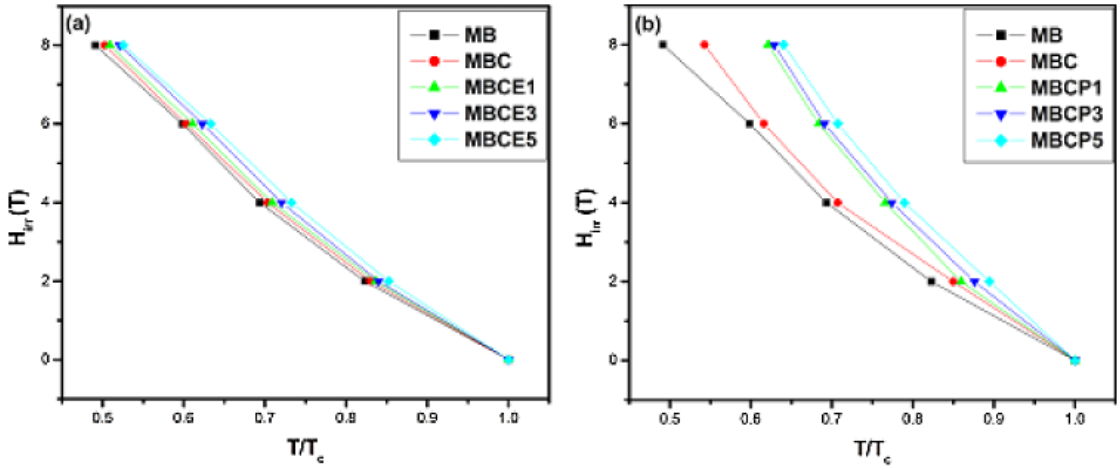

Figure 5. $H_{irr}(T)$ versus T/T_c curves of undoped and co-doped MgB_2 samples.

with a maximum value of f_p at $h = 0.2$ [57, 58], and the f_p versus h curves overlap if a single pinning mechanism is involved. In our case the f_p versus h curves do not overlap and the maximum values of f_p occur for h_{max} varying in the range 0.13–0.20 (see figure 7); this suggests that there is more than one pinning mechanism involved in the samples. Further, the value of h_{max} increases with an increasing doping level of rare earth oxide in the samples. It can be seen from figure 7 that the values of f_p for h varying in the range 0.4–0.7 have higher values for co-doped samples as compared to those of MB and MBC. This may be explained in terms of two grain boundary pinning factors: grain size and the dirtiness of the superconducting matrix. It has been pointed out that electron scattering pinning at the grain boundary (known as δk pinning) is strongly dependent upon the purity of the sample [59]. From the XRD results we have seen that crystallinity decreases, and lattice distortion increases, with increasing doping concentration in the samples, which results in enhanced grain boundary flux pinning. Further, nanosized impurity phases such as MgO, unreacted C and other impurity phases (EuB_6/PrB_6) present in the doped samples act as point pinning centers, leading to a slight improvement in their $J_c(H)$ values.

4. Conclusions

In summary, we have investigated the effect of REO and C co-doping on the superconducting properties of MgB_2 produced by the solid state reaction method. The decrease in T_c value with increasing doping level is due to enhanced lattice distortion in the doped samples. Improvements in the H_{c2} and H_{irr} of co-doped samples have been observed as compared to samples MB and MBC. In the case of Eu_2O_3 co-doped samples at 10 K a very small improvement in a high field ($>$6.5 T) $J_c(H)$ of sample MBCE1, and at 20 K a moderate improvement in a high field ($>$6 T) $J_c(H)$ of samples MBCE1 and MBCE3 as compared to the $J_c(H)$ value of sample MBC at respective temperatures have been observed. In the case of Pr_6O_{11} co-doped samples, however, a slightly greater increase in a high field ($> 6.5T$) $J_c(H)$ at 10 K of samples MBCP1 and MBCP3, and at 20 K only a marginal improvement in a high field ($>$ 6 T) $J_c(H)$ of sample MBCP1 as compared to the $J_c(H)$ value of sample MBC at respective temperatures have been observed. The enhancement of the H_{c2} and H_{irr} of co-doped samples is due to the introduction of impurity scattering centers in the MgB_2 lattice. The improvement in the high field

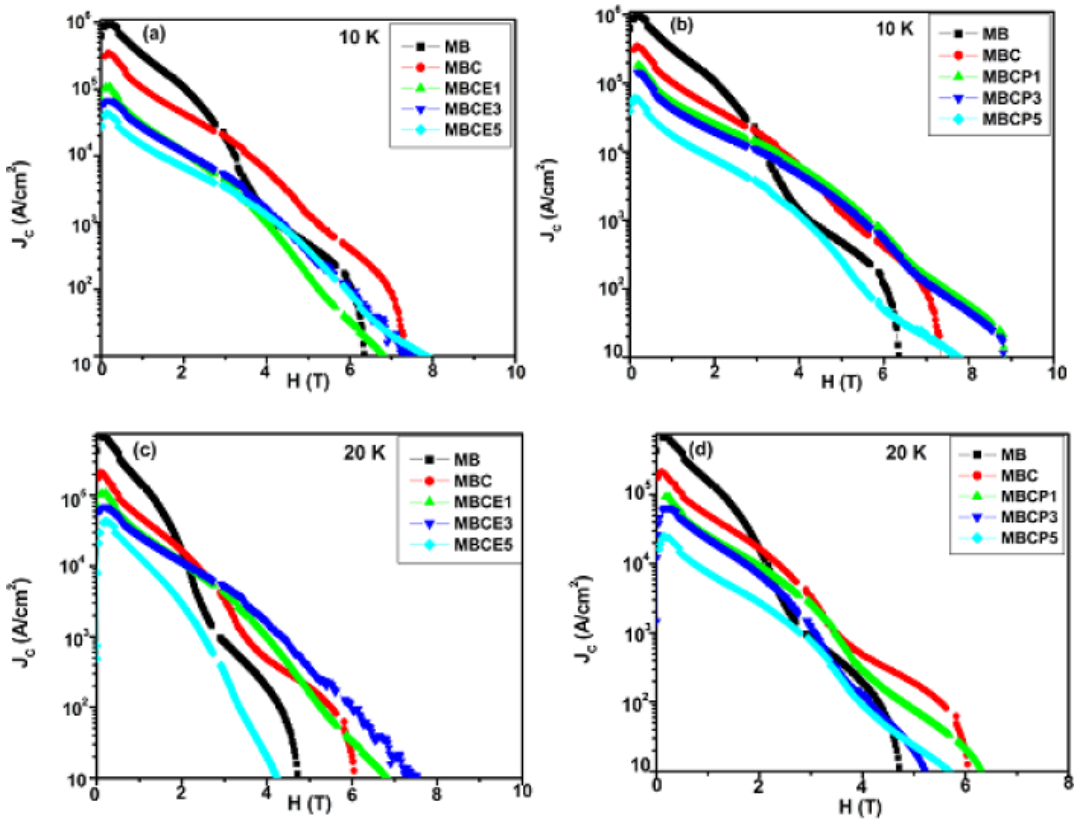

Figure 6. $J_c(H)$ versus $H(T)$ plots of undoped and co-doped MgB_2 samples measured at 10 and 20 K.

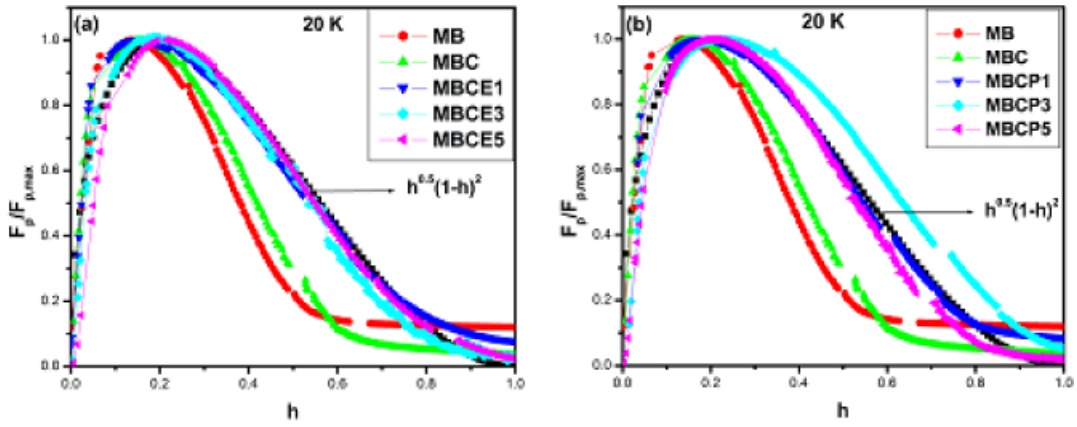

Figure 7. $F_p/F_{p,max}$ versus reduced field (h) plots at 20 K of undoped and co-doped MgB_2 samples.

$J_c(H)$ of some co-doped samples is due to the presence of impurity phases and lattice distortions.

Acknowledgments

This work was financially supported by DST (Govt. of India) and C.S.I.R. (Govt. of India). We wish to thank Dr R Rawat (UGC-DAE CSR, Indore Centre) for carrying out R–T measurements in a magnetic field.

References

[1] Larbalestier D, Gurevich A, Feldmann D M and Polyanskii A 2001 *Nature* **414** 368

[2] Buzea C and Yamashita T 2001 *Supercond. Sci. Technol.* **14** R115

[3] Naito M and Ueda K 2004 *Supercond. Sci. Technol.* **17** R1

[4] Serquis A *et al* 2002 *J. Appl. Phys.* **92** 351

[5] Liao X Z, Serquis A, Zhu Y T, Huang J Y, Civale L, Peterson D E, Xu H F and Mueller F M 2003 *J. Appl. Phys.* **93** 6208

[6] Dou S X, Soltanian S, Horvat J, Wang X L, Munroe P, Zhou S H, Ionescu M, Liu H K and Tomsic M 2002 *Appl. Phys. Lett.* **81** 3419

[7] Zhou S H, Pan A V, Qin M J, Liu H K and Dou S X 2003 *Physica* C **387** 321

[8] Berenov A, Serquis A, Liao X Z, Zhu Y T, Peterson D E, Bugoslavsky Y, Yates K A, Blamire M G, Cohen L F and MacManus-Driscoll J L 2004 *Supercond. Sci. Technol.* **17** 1093

[9] Chen S K, Wei M and MacManus-Driscoll J L 2006 *Appl. Phys. Lett.* **88** 192512
[10] Dou S X, Yeoh W K, Horvat J and Ionescu M 2003 *Appl. Phys. Lett.* **83** 4996
[11] Yeoh W K, Horvat J, Dou S X and Munroe P 2005 *IEEE Trans. Appl. Supercond.* **15** 3284
[12] Yeoh W K, Kim J H, Horvat J, Dou S X and Munroe P 2006 *Supercond. Sci. Technol.* **19** L5
[13] Kumakura H, Kitaguchi H, Matsumoto A and Hatakeyama H 2005 *IEEE Trans. Appl. Supercond.* **15** 3184
[14] Soltanian S, Wang X L, Horvat J, Dou S X, Sumption M D, Bhatia M, Collings E, Munroe P and Tomsic M 2005 *Supercond. Sci. Technol.* **18** 658
[15] Yamamoto A, Shimoyama J, Ueda S, Katsura Y, Horii S and Kishio K 2005 *IEEE Trans. Appl. Supercond.* **15** 3292
[16] Yan S C, Yan G, Lu Y F and Zhou L 2007 *Supercond. Sci. Technol.* **20** 549
[17] Ma Y W, Zhang X P, Nishijima J, Watanabe K, Awaji S and Bai X D 2006 *Appl. Phys. Lett.* **88** 072502
[18] Wilke R H T, Bud'ko S L, Canfield P C, Finnemore D K, Suplinskas R J and Hannahs S T 2004 *Phys. Rev. Lett.* **92** 217003
[19] Yeoh W K, Kim J H, Horvat J, Xu X and Dou S X 2007 *Physica* C **460** 568
[20] Yan S C, Yan G, Zhou L, Jia Y, Wen H H and Lu Y F 2007 *Supercond. Sci. Technol.* **20** 377
[21] Mickelson W, Cumings J, Han W Q and Zettl A 2002 *Phys. Rev.* B **65** 052505
[22] Yamamoto A, Shimoyama J, Ueda S, Iwayama I, Horii S and Kishio K 2005 *Supercond. Sci. Technol.* **18** 1323
[23] Kim J H, Zhou S, Hossain M S A, Pan A V and Dou S X 2006 *Appl. Phys. Lett.* **89** 142505
[24] Jun B H and Kim C J 2007 *Supercond. Sci. Technol.* **20** 980
[25] Kim J H, Xu X, Hossain M S A, Shi D Q, Zhao Y, Wang X L, Dou S X, Choi S and Kiyoshi T 2008 *Appl. Phys. Lett.* **92** 042506
[26] Shcherbakova O V, Pan A V, Wang J L, Shcherbakov A V, Dou S X, Wexler D, Babi'c E, Jerčinović M and Husnjak O 2008 *Supercond. Sci. Technol.* **21** 015005
[27] Vajpayee A, Awana V P S, Bhalla A N, Bhope P A, Nigam A K and Kishan H 2009 *Supercond. Sci. Technol.* **22** 015016
[28] Zeng R, Lu L and Dou S X 2008 *Supercond. Sci. Technol.* **21** 085003
[29] Flükiger R, Lezza P, Cesaretti M, Senatore C and Gladyshevskii R 2007 *IEEE Trans. Appl. Supercond.* **17** 2846
[30] Vinod K, Neson V, Syamaprasad U, Shipra and Sundaresan A 2008 *Supercond. Sci. Technol.* **21** 025003
[31] Wang J, Bugoslavsky Y, Berenov A, Cowey L, Caplin A D, Cohen L F, Driscoll J L M M, Cooley L D, Song X and Larbalestier D C 2002 *Appl. Phys. Lett.* **81** 2026
[32] Cheng C and Zhao Y 2006 *Appl. Phys. Lett.* **89** 252501
[33] Pan X F, Shen T M, Li G, Cheng C H and Zhao Y 2007 *Phys. Status Solidi* a **204** 1555
[34] Ojha N, Malik V K, Bernhard C and Varma G D 2009 *Physica* C **469** 846
[35] Ojha N, Malik V K, Bernhard C and Varma G D 2009 *Phys. Status Solidi* a **1** doi:10.1002/pssa.200925180
[36] Ojha N, Varma G D, Singh H K and Awana V P S 2009 *J. Appl. Phys.* **105** 07E315
[37] Paranthaman M, Thompson J R and Christen D K 2001 *Physica* C **355** 1
[38] Takenobu T, Ito T, Chi D H, Prassides K and Iwasa Y 2001 *Phys. Rev.* B **64** 134513
[39] Zhang X, Ma Y, Gao Z, Wang D, Yu Z and Wang L 2007 *Supercond. Sci. Technol.* **20** 1198
[40] Beans C P 1964 *Rev. Mod. Phys.* **36** 31
[41] Yeoh W K, Kim J H, Horvat J, Xu X, Qin M J, Dou S X, Jiang C H, Nakane T, Kumakura H and Munroe P 2006 *Supercond. Sci. Technol.* **19** 596
[42] Williamson G K and Hall W H 1953 *Acta Metall.* **1** 22
[43] Liao X Z, Serquis A, Zhu Y T, Peterson D E, Mueller F M and Xu H F 2004 *Supercond. Sci. Technol.* **17** 1026
[44] Kim J H, Dou S X, Sangjun Oh, Jerčinović M, Babić E, Nakane T and Kumakura H 2008 *J. Appl. Phys.* **104** 063911
[45] Kim J H, Oh S, Xu X, Joo J, Rindfleisch M, Tomsic M and Dou S X 2009 *J. Nanosci. Nanotechnol.* **9** 7477
[46] Sequis A, Zhu Y T, Peterson E J, Coulter J Y, Peterson D E and Mueller F M 2001 *Appl. Phys. Lett.* **79** 4399
[47] Rowell J M 2003 *Supercond. Sci. Technol.* **16** R17
[48] Canfield C, Finnemore D K, Bud'ko S L, Ostenson J E, Lapertot G, Cunningham C E and Petrovic C 2001 *Phys. Rev. Lett.* **86** 2423
[49] Zhang Y, Zhou S H, Lu C, Konstantinov K and Dou S X 2009 *Supercond. Sci. Technol.* **22** 015025
[50] Matsumoto A, Kitaguchi H and Kumakura H 2008 *Supercond. Sci. Technol.* **21** 065007
[51] Vinod K, Neson V, Roy S B and Syamaprasad U 2009 *Supercond. Sci. Technol.* **22** 055009
[52] Vajpayee A, Awana V P S, Bhalla G L and Kishan H 2008 *Nanotechnology* **19** 125708
[53] Zhang X, Wang D, Gao Z, Wang L, Ma Y, Qi Z and Watanabe K 2008 *Supercond. Sci. Technol.* **21** 075008
[54] Dou S X, Braccini V, Soltanian S, Klie R, Zhu Y, Li S, Wang X L and Larbalestier D 2004 *J. Appl. Phys.* **96** 7549
[55] Yamamoto A, Shimoyama J, Ueda S, Katsura Y, Iwayama I, Horii S and Kishio K 2005 *Appl. Phy. Lett.* **86** 212502
[56] Serquis A, Serrano G, Moreno S M, Civale L, Maiorov B, Balakirev F and Jaime M 2007 *Supercond. Sci. Technol.* **20** L12
[57] Dew-Huges D 1987 *Phil. Mag.* B **55** 459
[58] Tarantini C *et al* 2007 *Physica* C **463** 211
[59] Cheng C H, Yang Y, Munroe P and Zhao Y 2007 *Supercond. Sci. Technol.* **20** 296